LANGMUIR

Article

Spatially Resolved Monitoring of Drying of Hierarchical Porous Organic Networks.

Manuel Isaac Velasco, Emilia V. Silletta, Cesar G. Gomez, Miriam C. Strumia, Siegfried Stapf, Gustavo Alberto Monti, Carlos Mattea, and Rodolfo H. Acosta

Langmuir, **Just Accepted Manuscript** • DOI: 10.1021/acs.langmuir.5b04230 • Publication Date (Web): 05 Feb 2016

ACS Publications

Langmuir is published by the American Chemical Society. 1155 Sixteenth Street N.W., Washington, DC 20036

Spatially Resolved Monitoring of Drying of Hierarchical Porous Organic Networks

Velasco, Manuel Isaac [a], Silletta, Emilia V. [a], Gomez, Cesar G. [b], Strumia, Miriam C.[b], Stapf, Siegfried [c], Monti, Gustavo Alberto [a], Mattea, Carlos [c], Acosta, Rodolfo H. [a]*

a) FaMAF-Universidad Nacional de Córdoba and IFEG-CONICET, 5000 Córdoba, Argentina.

b) Departamento de Química Orgánica, Facultad de Ciencias Químicas, (IMBIV-CONICET) Universidad Nacional de Córdoba, Haya de la Torre y Medina Allende, Edificio de Ciencias II - Ciudad Universitaria, 5000 Córdoba, Argentina

c) Ilmenau University of Technology, Department of Technical Physics II/Polymer Physics, 98684 Ilmenau, Germany

Abstract

Evaporation kinetics of water confined in hierarchal polymeric porous media is studied by low field nuclear magnetic resonance (NMR). Systems synthesized with various degrees of crosslinker density render networks with similar pore sizes but different response when soaked with water. Polymeric networks with low percentage of crosslinker can undergo swelling, which affects the porosity as well as the drying kinetics. The drying process is monitored macroscopically by single-sided NMR, with spatial resolution of 100 μm, while microscopic information is obtained by measurements of spin-spin relaxation times (T_2). Transition from a funicular to a pendular regime, where hydraulic connectivity is lost and the capillary flow cannot compensate the surface evaporation, can be observed from inspection of the water content in different sample layers. Relaxation measurements indicate that even when the larger pore structures are depleted of water, capillary flow occurs through smaller voids.

1. Introduction

Porous systems are spread in a wide variety of materials in nature, everyday life or more complex technological applications. Due to their relevance, scientists have studied these materials from different approaches, for instance, polymeric matrices used in chromatography,[1] gas sorption or as a catalyst support.[2] Macroporous adsorption resins are porous cross-linked polymer beads that have been developed as useful adsorbents. They have shown high physical and chemical stabilities, large specific surface area, high adsorption capacities, easy regeneration, and long service life.[3] Pore architecture leads to effective separation and reorientation of fluid elements, creating a high interfacial area between the immiscible phases for mass transfer to occur in liquid-liquid extraction.[4] The hierarchy and material pore architecture as well as the fluid contained inside the pores can be optimized to reach a successful performance for a given application. As expected, the structure and pore accessibility play the main role in the dynamics which a fluid can undergo in confinement. In addition, the liquid in the pore may be in a stagnant state -e.g. water or oil in a rock reservoir- or may flow through the pores system. Among several events that take place when the liquid phase flows, the drying process of organic porous materials is one of the most complex ones.[5] The dynamics of water transport during its evaporation from a porous material depends on several parameters, such as the average size and pore distribution, physicochemical interactions between the liquid and the solid matrix, the external environment conditions and others. Additionally, some organic porous materials may also shrink during the liquid evaporation, leading to the addition of another variable to the study.

A considerable amount of effort has been channelled into the development of theoretical models that can accurately predict the behaviour of fluids in porous systems during drying.[6–10] More complex and sophisticated models have been developed from increased use of computational resources and the growing interest in the oil industry.[8,11,12] Simulations can be carried out by computing the flow and transport equations either in a simplified topologically modelled

network or on topological representation of a network obtained by imaging the pore architecture.[13] Among the experimental reports, gravimetric studies,[5] photography and neutron transmission spectroscopy[14] are the most used to study the drying process. To a lesser extent, Nuclear Magnetic Resonance (NMR) and Magnetic resonance Imaging (MRI) have been also employed to examine the drying phenomena.[15–17] These are mainly focused on inorganic rigid matrices such as sand or concrete.[11,18–20] Surprisingly, there are no reports to our knowledge on the drying of stable porous polymeric materials, although they have found a wide spectrum of applications such as support for catalysts,[21] immobilization of enzymes,[22] HPLC columns, adsorbent devices and release of active substances,[23] among others.[24] The lack of reports may be attributed to the complexity of the study since deswelling or shrinkage in the organic network may also take place during the drying process.

A study of evaporation from a bulk material by means of the NMR signal of the liquid inside the pore structure was previously reported.[25] Those results showed that the pore architecture of polymeric porous beads, synthesized with a lower crosslinking degree, differs from dry to soaked state due to the liquid-matrix interaction. Monitoring the behaviour of of water contained in different pore size distributions during the evaporation as well as the deswelling dynamics, internal migration of water between pores of different sizes was evidenced. Therefore, the drying of polymeric materials with a hierarchical pore structure was showed to proceed in a hierarchical way. Moreover, it would be expected that this event takes place anisotropically since the evaporation rate is a function of the surface evaporation, mainly from the sample surface exposed to air.

The study of spatial slices of the sample can be achieved with the Profile NMR-MOUSE® (MObile Universal Surface Explorer), a portable open NMR sensor equipped with a permanent magnet geometry that generates a well-defined flat sensitive volume parallel to the scanner surface.[26,27] To excite and detect the NMR signal of this volume, a surface radiofrequency (RF) coil is placed on top of the magnet at a position that defines the maximum penetration into the sample. As the sensitive slice is repositioned across the object, this unilateral NMR scanner produces one-dimensional profiles of the sample structure with a spatial resolution of up to 10

μm. The NMR–MOUSE has been successfully employed in diverse studies such as velocity determinations, MRI, spectroscopic characterization and relaxometry, among others.[28–33]

The aim of this study is to analyse the evaporation of water in porous polymeric matrices using the NMR–MOUSE to understand the dynamic phenomena that may take place during the process. First we will describe how single–sided NMR could be used to monitor an evaporation process and the management of data to establish different drying regimes during the evaporation. Finally, data will be combined with relaxation measurements to examine the influence of the pore structure on water distribution into pore architecture during drying.

2. Theoretical background

2.1 Drying kinetics

Drying curves in porous media are expected to show different evaporation periods, as schematized in Fig. 1.[9,34] The first period known as initial drying period (IDP) or surface evaporation regime (SER), where the evaporation occurs from the surface of the most external mass of liquid and is associated with a rapid drop in the drying rate. This is followed by the constant rate (CRP) and falling rate period (FRP). In CRP the evaporation continues to be from the upper layer while liquid is removed from the main body of the porous medium by internal capillary flow through hydraulic connections among pores. This process is rapid enough to balance the rate of water removal at the surface. The regime of internally connected capillary liquid flow is also known as the funicular regime.[35] FRP starts when a percolation threshold is reached and the water surface breaks into patches. In this period, drying is mainly governed by mass transfer through the dry pore space. The fourth stage is characterized by the receding of the drying front (RFP), where a dry region develops close to the open side and a two-phase region away from it.[3] In addition; two typical events can be described from these four stages. One of them is the main cluster disconnection (MCD), which occurs when the liquid cluster loses contact with the open side of the pore network. The second remarkable event is the breakthrough (BT) that occurs when a dry region is developed in the bottom of the sample.

As expected, the morphological aspect of the porous matrix plays a main role in the dynamics of drying. Consequently the appearance, duration and the order of all these events and regimes are closely associated with pore parameters: size, shape, connectivity and hydrophobicity among others[36]; and drying conditions: open boundaries, gas flow conditions, heat transfer, sample disposal, etc.[37] In complex porous systems it is not always possible to determine precisely all these processes from an integral evaporation curve. Therefore the spatial resolution is essential for the determination of the evaporation dynamics, where it is clear that the acquisition time of the experimental technique must enable a time resolution such that no significant variation in the average dynamics takes place while a single image is detected.

2.2 Spatially resolved study of water content during drying

Single–sided NMR sensors offer access to study arbitrarily sized objects in a non-invasive way. They combine open magnets and surface radiofrequency (RF) coils to generate a sensitive volume external to the sensor and inside the object under investigation.[2] The NMR–MOUSE provides depth resolutions in the range of 10–100 μm. It takes advantage of a simple magnet geometry that generates a magnetic field with an extremely uniform gradient to resolve the structure near surface of samples. The scanning procedure requires repositioning the sensor, which is equipped with a low inductance RF coil that is insensitive to loading changes during the scanning procedure avoiding the necessity of retuning. The definition of a flat sensitive volume is advantageous in the study of thin samples, where an important sensitivity improvement is expected from the larger intersection of the sample and the sensitive volume. Furthermore, background signals from the sensor housing are completely eliminated.

The most standard technique for measuring the decay of time domain signals in this type of devices is with a multipulse, Carr-Purcell-Meiboom-Gill (CPMG) sequence, in which an initial 90º RF excitation pulse is followed by successive 180º refocusing pulses that generate a train of echoes. The intensity of the signal at each penetration depth (S_d) corresponding to the top of the echoes during an evaporation process can be described as:[38]

$$S_d(m\tau, t) = A(d,t)e^{\left\{-\left(\frac{1}{T_2}+\frac{1}{12}(\gamma G_0 \tau)^2 D\right)m\tau\right\}} \quad (1)$$

where T_2 is the transversal relaxation, γ the gyromagnetic ratio, G_0 is the gradient of the magnetic field, τ is the echo time, *m* the echo number, *D* diffusion constant of water and *t* the evaporation time. Here the assumption is that no significant evaporation is undergoing during the acquisition of the NMR signal, thus both the relaxation time and the diffusion coefficient are independent of *t.* The coefficient $A(d,t)$is proportional to the amount of water at a given instant of time in a sample layer located at a distance *d* from the surface of the NMR-MOUSE.

To follow the evaporation kinetics with the surface explorer, a CPMG signal is acquired in every slice and $A(d,t)$ is plotted as a function of the scanning depth, obtaining a so-called sample profile. Figure 2 shows a schematic representation of the expected profile during different drying dynamics. For instance, if evaporation starts from the top of the sample, the signal arising from these slices decrease while the bottom ones remain unchanged. From this profile plots, the evaporation front position (FP) at different times can be determined (Fig. 2a). On the other hand, if a fluid evaporates from the porous system evenly, the signal stemming from all the slices will reduce in intensity without modifying the front position (Fig. 2b). In particular, a change in the intensity of the bottom slice shows the BT, and the instant of time when the signal of the top slice is negligible would indicate the MCD.

2.3 Relaxation

Additional information could in principle be extracted from the rate of the exponential decay in Eq. (1). Brownstein and Tarr[39,40] demonstrated that relaxation times of a confined liquid are proportional to the surface to volume ratio (S/V) of the confining pore in the case that the pore is completely filled with the liquid. If the magnetization decay can be considered to be dominated entirely by the interaction of individual spins with the pore wall, given by a surface relaxation parameter ρ, where the molecular diffusion will be the driving mechanism, then relaxation follows the relation $T_2^{-1} = \rho\, S/V$. In systems with a high dispersion in pore sizes the CPMG sequence is expected to present a multi-exponential decay, which can readily be used to

characterize properties from a liquid confined in each void size.[41] In a previous study we determined that the relaxation times in an homogeneous magnetic field of 1.4 T are in the order of 800 ms for water contained in the large pores (P1) and 40 ms for water contained between the microspheres (P2).[25] The extremely high values of magnetic field gradient of the NMR-MOUSE hinder this observation, especially for liquid confined in large pores, where long T_2 values are obtained. In this case, the term with the static gradient in Eq. (1) will dominate the relaxation measurement. For this reason, in this work we correlate information obtained in a relaxometer with a homogeneous magnetic field with that attained from profiles acquired with the surface scanner.

3. Experimental

3.1 Polymeric network

The study was performed using polymer beads with hierarchical pore structure corresponding to copolymers of ethylene glycol dimethacrylate and 2-hydroxyethyl methacrylate [poly(EGDMA-co-HEMA)] synthesized as previously reported.[42] For the suspension polymerization reaction cyclohexane was used as a porogenic agent, PVP as a suspension stabilizer and BPO was used as a radical initiator. Different polymeric networks were obtained varying the crosslinker content with 6, 10, 17, 25 and 33 mol% of EGDMA. The resulting system resembles a powder, which presents hierarchically distributed pore sizes. These systems are highly stable; maintaining the pore structure even in the dry state. Polymer beads that contain large agglomerates of microspheres (100-200 nm) are formed. Each microsphere consists in turn of smaller nuclei (10–20 nm) which are nonporous and represent the most highly cross-linked regions of the system. The nuclei are blended to some extent where the inter-space between them gives rise to small cavities, which are mainly responsible for the high surface to volume ratio of this type of material. We have previously reported that three to four different pore size groups can be determined by NMR relaxation measurements in homogeneous magnetic field.[23] Large pores (P_1) are generated when the microspheres are agglomerated into larger irregular entities in the polymer material (10 μm –400 μm) with relaxation values close to bulk water,

i.e.~ 1 sec. Water contained in the space between the microspheres (P_2) renders $T_2 \sim 40$ ms, while relaxation values for bound, or adsorbed water are in the order of 1 ms. Samples with higher percentage of cross–linker have shown to render a more stable pore structure, even when soaked with polar liquids such as water. For lower content of EGDMA, an appreciable degree of expansion of the polymer mesh occurs, giving rise to a soft network (gel fraction) that partially collapses giving rise to smaller intermediate void sizes. Networks prepared with a 6 and 10 mol% of EGDMA content have a water population with a T_2 relaxation time of ~ 200 ms. Monitoring changes in relaxation times during the drying process have shown that water migration is produced between the gel fraction of the matrix and P_2. Additionally, at room temperature and pressure, water in smaller voids, which is tightly bound to the mesh, does not evaporate.[23]

3.2 Single-sided NMR

In this work, an NMR-MOUSE PM25 (ACT GmbH, Aachen, Germany) was used. The device has an accessible vertical range of 25 mm, the resonance frequency for ^{1}H is 11.7 MHz and it has a static gradient of 11.5 T/m. For this device, the slice thickness was set as 100 μm. Samples were soaked in water overnight to reach a fully saturated state. A portion of the sample was distributed in a 50 mm diameter plastic Petri dish in order to obtain a flat layer of sample approximately 1.5 mm in height. Excess water was removed using an adsorbent paper before starting the NMR experiment. Samples were allowed to dry at room temperature (25 ºC) and several transverse proton relaxation times were measured throughout the drying process by using a Carr-Purcell-Meiboom-Gill (CPMG)[43] sequence. A number of 1024 echoes were acquired with an echo time τ of 80.75 μs. In every experiment, 128 scans were averaged in order to improve the signal to noise ratio. CPMG experiments were acquired at 14 different sample heights starting from the upper part, with an acquisition time of 75 s for each layer. Immediately after the entire sample thickness is scanned, the initial position is restored and

another experiment is started. The necessary time to explore the whole sample was approximately 23 minutes. A total evaporation time of ca. 5 hours was monitored.

3.3 Relaxation experiments in homogeneous field

Relaxation measurements in homogeneous magnetic fields were carried out following the protocol described previously.[25] Samples soaked overnight were gently placed in a 5 mm outer diameter NMR sample tube, which was cut to a length of 10 mm to allow proper evaporation. Experiments were carried out at 25 ºC at a magnetic field corresponding to 60 MHz for ^{1}H, using a permanent magnet (Varian EM360) and a Kea2 spectrometer (Magritek, Wellington, New Zealand). A CPMG sequence with echo time of 1 ms and 6000 echoes was used, with eight scans for each experiment. A total period of 25 h was monitored; with an acquisition of a relaxation curve every 15 min. Relaxation decays were deconvoluted using a numerical Inverse Laplace Transform software provided by P. Galvosas (University of Wellington, New Zealand).

4. Results and discussion

4.1 Water uptake and overall evaporation

A representative profile of a sample prepared with a 33 mol % of EGDMA content before the beginning of evaporation is shown in Fig. 3a. The slice located at the bottom of the sample corresponds to d = 0.75 mm, while the top slice appears at d = 1.95 mm, where d is the distance measured from the scanner's surface. All further description is carried out considering a variable h defined such that $h = 0$ describes the slice of the sample closest to the magnet, or sample bottom slice. The signal intensity for each slice is proportional to the amount of confined water in this volume, and is represented in this case by $A(h, 0)$. It is worth noting that as data are acquired with a CPMG sequence, the signal arising from protons of the polymer mesh are not detected as the relaxation time of these protons is shorter than the echo time. A measure of the water uptake of each network can be defined as the amount of water present in the bottom layer of the soaked sample, $A(0,0)$.

The effect of expansion of the matrix mesh can be clearly observed in Fig. 3b, where samples with a 6 and 10 mol% of EGDMA content have higher signal intensity due to the larger amount of water present in the bottom slice. The time decay of the overall NMR signal is analogue to the evaporation kinetics followed by a gravimetric experiment. Since samples have different amount of water, a comparison of the drying kinetics can be carried out by inspection of the time evolution of a normalized water content, which is defined as:

$$nW_c(t) = \frac{\sum_i A(i,t)}{\sum_i A(i,0)}, \quad (2)$$

where i indicates the slice number. Figure 3c shows the evolution of the normalized water content for samples with a 6 and 33 mol % of EGDMA content. No significant difference is observed until the final drying stage; however detailed information on the evaporation kinetics can be obtained by inspection of individual slices, as shown below.

4.2 Spatially resolved water content during drying

Figure 4 shows the evolution of the profiles during the drying of samples with different crosslinking degrees. All experiments were repeated several times with slightly different sample heights and no significant change in the evaporation dynamics was observed. Samples with EGDMA content higher than a 17 mol % are observed to dry in a similar way (Fig. 4 a,b). Initially, a decrease in the signal intensity occurs evenly throughout all samples as is sketched in Fig. 2b, indicating a redistribution of water through all the porous media. Towards the end of the evaporation, the signal of lower slices decreases with a faster rate than that found for the top. On the other hand, in early stages of evaporation, swollen networks (6 and 10 mol % of EGDMA, in Fig. 4 d,e) show an intensity gradient through the where the bottom of the sample has a larger amount of water as compared to the top. This effect is related to the ability of these systems to undergo swelling. In this situation a layer of gel is present through the pores surface. Water molecules in the gel fraction present two distinct sets of mobility, a low one for water molecules strongly bounded with the polymer chains via hydrogen bond, and a higher one driven by self-diffusion of molecules contained inside the gel fraction. This change in mobility

with respect to water molecules contained within the pore network affects the dynamics of the funicular regime as discussed further. Additionally, swelling renders softer polymer networks that undergo deformations that change the pore space distribution. Variations in porosity from 84 % for networks with 33 % EGDMA to 66 % for those with 6 % EGDMA have been reported.[42] After significant water evaporation the profiles resemble the initial ones of the non-swollen samples, in which the water content is evenly distributed. As will be shown below, this event corresponds to the deswelling of the polymer matrix. Samples prepared with 17 % of EGDMA, are expected to be similar to those with high cross–linking, however they share similarities with the swollen samples.

The drying kinetics can be better described by observing changes in the water content for representative slices as a function of time. Data for highly cross-linked networks (33 % EGDMA content) are shown in Fig. 5a. For a slice far away from the bottom of the sample (S3) the signal intensity is zero as there is no water present above the sample, the following slice (S4) is at the air/polymer interface, thus the initial data have a low value and vanishes rapidly. The following slice (S5) is assigned to water fully contained in the pore network. A rapid decay in the signal intensity of this slice is followed by a stabilization period, a plateau in which the surface saturation remains constant. The following slice (S6), 150 μm deeper into the sample, has constant water content during most of the rapid decay of S5. Correspondingly, the signal intensity at the bottom (S13) remains constant during the whole initial decay period of S5. As the plateau for the surface saturation is reached, the amount of water at the bottom of the sample monotonically decays until a crossover with the signal intensity of the slice corresponding to the top is observed. The final evaporation of sample surface (both S5 and S6) occurs after no remaining water is present at the bottom. The abrupt change in the dynamics of water content between S5 and S6 in the early evaporation stages is reflected by the square shape of the profiles shown in Fig. 4a. This is not the case for softer networks where a gradual transition is obtained. Figure 5b shows the time dependence of the water content for networks prepared with 6 % of EGDMA content. Slice S1 corresponds to air while S2 is the slice that includes the air/polymer interface, however, this sample portion does not dry in the same fashion as the

previously described network, but rather maintains a small degree of water during the whole process. Deeper into the sample (S4) an initial rapid decay is observed, followed by a low drying rate period, which is not a defined plateau as observed before. The following slice (S5) presents a constant decay ratio which is maintained until the water content in the bottom slice (S13) is drastically reduced. A main cluster disconnection is not observed for either sample. From Fig. 5a the drying front position could be defined either at the sample top (S5) or bottom (S13) by observing which of these slices change its water content, thus a shift of the FP would be present at the beginning of the plateau for S5. This definition cannot be applied to swollen networks as is has been observed that a monotonic decay from all parts of the sample is present during the drying process.

The initial rapid decay on the surface saturation may be due to a faster evaporation rate from those pores closer to the surface, where the influence of gravity is stronger than the capillary effect. After that, a critical coexistence in the liquid-vapour relation is reached within the detected slice volume. During the constant period of surface saturation the liquid film covering the pores most probably spans through the whole sample, that is, a main liquid cluster which provides hydraulic connectivity across the entire pore network is developed, corresponding to a funicular regime. Numerical simulations indicate that during the early evaporation stage, a small number of disconnected water clusters are present, and the main liquid cluster covers the major part of the evaporation boundary.[9,34] As evaporation continues, water is transported in the form of viscous flow through the main liquid cluster, which provides the necessary water mass to maintain a stable evaporating front. The amount of water on the surface that the system can retain during this period depends on the cross-linker content. The quantity $\mathrm{nSS} = A(\mathrm{TS}, t_p)/A(0,0)$, represents a normalized surface saturation, where the signal intensity from the surface layer is expressed relative to the capability of the system's water uptake. TS stands for the top slice and t_p the instant of time when the plateau is reached. It has been previously reported that the pore volume changes with the cross-linker content showing a maximum variation in pore size for a 17 mol % of EGDMA.[25,42] Networks with a 33 mol% of EGDMA are the more stable ones presenting small changes in the pore size upon saturation with water, while those networks

with a 6 mol % of EGDMA show a negative change in the pore size, that is, these softer networks undergo deformation upon mesh expansion rendering an overall smaller void size. In other words, during the constant surface saturation period, the amount of water retained on the surface appears to follow the tendency of the pore size variation (Fig. 6a).[42] A precise determination of the dimensions of the different pores and the relation with the amount of water retained on the surface is a complex problem that is subject to further studies.

The time in which the vapour phase reaches the bottom of the sample, or t_{BT}, is also dependent on the pore size, although to a lesser extent (Fig. 6b). An appropriate measure of time used for comparison of different systems is the liquid saturation (LS). A value of LS=1 represents the initial instant of time when the system is fully saturated, and LS=0 indicates the time when the evaporation process is concluded, thus, BT(LS) indicates the time when the breakthrough takes place in units of liquid saturation and corresponds to an instant of time where LS(h=0) < 1, corresponding to the bottom slice (S13). Here it must be taken into account that the sensitive volume corresponds to a 100 μm slice with an area of (4 × 4) mm^2. Samples with a content of 6 and 33 mol % of EGDMA content are expected to have a similar pore size as the relaxation times for the dominating pores (P2) present similar relaxation time values of approximately 40 ms; however BT is delayed in the former one. This is most probably due to water migration from the swollen polymer (external gel fraction) into the pore network.[25]

4.3 Microscopic water distribution during drying

To explore the evaporation kinetics the liquid content of top (S5) and bottom (S13) slices as a function of the liquid content for networks with 33 % of EGDMA content are compared (see Fig. 7) with the amount of water obtained for each cavity size as determined by relaxation measurements in a homogeneous magnetic field.[25] From the lower panel it can be observed that the evaporation is initially produced due to a reduction of the water content in larger cavities (P1) while the amount of water contained in smaller voids (P2) remains constant. The plateau for the water content in S5 is reached for LS = 0.85 and draining of the bottom slice starts. Even when large voids (P1) are completely depleted at LS = 0.45, the hydraulic connectivity seems to

be present as the amount of water in the surface remains constant, implying that the rate of water delivered to the surface by flow still compensates the evaporation rate. At this instant of time the overall amount of water in P2 starts to decay. At LS = 0.3 most probably the connectivity of the main water cluster is lost, and the pendular regime is reached. At this stage the bottom of the sample appear to be almost dry and evaporation from the top of the sample is observed.

The same analysis for samples prepared with 6 % of EGDMA content is shown in Fig. 8, where slices S4 and S13 are taken as representative for the top and bottom of the sample respectively. An initial fast decay of water contained in the top of the sample is observed until the liquid content reaches a value of LS = 0.92. This corresponds to an equilibration of the amount of water in the swollen mesh and decay of the water content in the large pores (P1). At LS = 0.6 water in P1 is completely drained and deswelling of the polymer mesh starts. After LS = 0.5 is reached, the water corresponding to the swollen mesh disappears, evaporation of water from P2 starts and the rate of water removal from S4 increases. Note that this is the time in which the profiles shown in Fig. 4e change from a gradient to a constant value with respect to the scanned depth. This most probably corresponds to a pendular regime, although a sharp transition is not to be expected due to the non-uniform release of water from the gel fraction.

In summary, we have shown that unilateral NMR combined with relaxation measurements is a promising protocol for the assessment of water dynamics during evaporation in organic porous polymers.

5. Conclusions

Single-sided NMR combined with relaxation data has proved to be exceedingly useful in the study of the evaporation dynamics in organic porous materials. The data obtained from this non-invasive and non-destructive method promises to be a very valuable tool that provides experimental data to complement theoretical and computational models proposed to fully characterise evaporation processes. Data from integral measurements such as gravimetric

methods or use of solely NMR relaxation are not able to provide the richness of information given by acquisition with spatial resolution.

Acknowledgments

We thank the financial support from CONICET, SeCyT Universidad Nacional de Córdoba, and ANPCYT PICT 2010-1096. M.I. Velasco thanks DAAD for the traveling fellowship.

References

(1) Gölgelioğlu, C.; Bayraktar, A.; Celebi, B.; Uğuzdoğan, E.; Tuncel, A. Aqueous Size Exclusion Chromatography in Semimicro and Micro-Columns by Newly Synthesized Monodisperse Macroporous Hydrophilic Beads as a Stationary Phase. *J. Chromatogr. A* **2012**, *1224*, 43–50.

(2) Davis, M. Ordered Porous Materials for Emerging Applications. *Nature* **2002**, *417* (June), 813–821.

(3) Wu, X.; Liu, Y.; Liu, Y.; Di, D. Evaluation on the Adsorption Capability of Chemically Modified Macroporous Adsorption Resin with Ionic Liquid. *Colloids Surfaces A Physicochem. Eng. Asp.* **2015**, *469*, 141–149.

(4) Tebboth, M.; Kogelbauer, A.; Bismarck, A. Liquid–Liquid Extraction within Emulsion Templated Macroporous Polymers. *Ind. Eng. Chem. Res.* **2015**, *54* (29), 7284–7291.

(5) Errede, L. A. Polymer Drying. IV. A Molecular Interpretation of Polymer Drying. *J. Polym. Sci. Part A Polym. Chem.* **1990**, *28* (4), 857–870.

(6) Le Bray, Y.; Prat, M. Three-Dimensional Pore Network Simulation of Drying in Capillary Porous Media. *Int. J. Heat Mass Transf.* **1999**, *42* (22), 4207–4224.

(7) Prat, M. Recent Advances in Pore-Scale Models for Drying of Porous Media. *Chem. Eng. J.* **2002**, *86* (5502), 153–164.

(8) Metzger, T.; Tsotsas, E. Network Models for Capillary Porous Media: Application to Drying Technology. *Chemie Ing. Tech.* **2010**, *82* (6), 869–879.

(9) Yiotis, A. G.; Tsimpanogiannis, I. N.; Stubos, A. K.; Yortsos, Y. C. Pore-Network Study of the Characteristic Periods in the Drying of Porous Materials. *J. Colloid Interface Sci.* **2006**, *297* (2), 738–748.

(10) Wu, R.; Cui, G. M.; Chen, R. Pore Network Study of Slow Evaporation in Hydrophobic Porous Media. *Int. J. Heat Mass Transf.* **2014**, *68*, 310–323.

(11) Shokri, N.; Or, D. Drying Patterns of Porous Media Containing Wettability Contrasts. *J. Colloid Interface Sci.* **2013**, *391*, 135–141.

(12) Prat, M.; Bouleux, F. Drying of Capillary Porous Media with a Stabilized Front in Two Dimensions. *Phys. Rev. E. Stat. Phys. Plasmas. Fluids. Relat. Interdiscip. Topics* **1999**, *60* (5), 5647–5656.

(13) Blunt, M. J.; Bijeljic, B.; Dong, H.; Gharbi, O.; Iglauer, S.; Mostaghimi, P.; Paluszny, A.; Pentland, C. Pore-Scale Imaging and Modelling. *Adv. Water Resour.* **2013**, *51*, 197–216.

(14) Lehmann, P.; Assouline, S.; Or, D. Characteristic Lengths Affecting Evaporative Drying of Porous Media. *Phys. Rev. E* **2008**, *77* (5), 056309.

(15) Harding, S. G.; Wessman, D.; Stenstrom, S.; Kenne, L. Water Transport during the Drying of Cardboard Studied by NMR Imaging and Diffusion Techniques. *Chem. Eng. Sci.* **2001**, *56*, 5269–5281.

(16) Williams, P. D.; Oztop, M. H.; McCarthy, M. J.; McCarthy, K. L.; Lo, Y. M. Characterization of Water Distribution in Xanthan-Curdlan Hydrogel Complex Using Magnetic Resonance Imaging, Nuclear Magnetic Resonance Relaxometry, Rheology, and Scanning Electron Microscopy. *J. Food Sci.* **2011**, *76* (6), E472–E478.

(17) Koptyug, I. V. MRI of Mass Transport in Porous Media: Drying and Sorption Processes. *Prog. Nucl. Magn. Reson. Spectrosc.* **2012**, *65*, 1–65.

(18) Laurindo, J. B.; Prat, M. Numerical and Experimental Network Study of Evaporation in Capillary Porous Media. Phase Distributions. *Chem. Eng. Sci.* **1996**, *51* (12), 5171–5185.

(19) Valckenborg, R. M. E.; Pel, L.; Hazrati, K.; Kopinga, K.; Marchand, J. Pore Water Distribution in Mortar during Drying as Determined by NMR. *Mater. Struct.* **2005**, *34* (244), 599–604.

(20) Shahraeeni, E.; Or, D. Pore-Scale Analysis of Evaporation and Condensation Dynamics in Porous Media. *Langmuir* **2010**, *26* (17), 13924–13936.

(21) Islam, S. M.; Tuhina, K.; Mubarak, M.; Mondal, P. Hydrogenation of Various Organic Substrates Using Polystyrene Anchored Orthometallated Ruthenium (II) Complex as Catalyst. *J. Mol. Catal. A Chem.* **2009**, *297* (1), 18–25.

(22) Dhake, K. P.; Bhatte, K. D.; Wagh, Y. S.; Singhal, R. S.; Bhanage, B. M. Immobilization of Steapsin Lipase on Macroporous Immobead-350 for Biodiesel Production in Solvent Free System. *Biotechnol. Bioprocess Eng.* **2012**, *17* (5), 959–965.

(23) Shaha, V.; Jain, H.; Krishna, J.; Patel, P. Microsponge Drug Delivery : A Review. *Int. J. Pharm. Sci.* **2010**, *1* (2), 212–218.

(24) Jiang, K.; Sposito, A.; Liu, J.; Raghavan, S. R.; Devoe, D. L. Microfluidic Synthesis of Macroporous Polymer Immunobeads. *Polymer (Guildf).* **2012**, *53*, 5469–5475.

(25) Silletta, E. V; Velasco, M. I.; Gómez, C. G.; Acosta, R. H.; Strumia, M. C.; Monti, G. a. Evaporation Kinetics in Swollen Porous Polymeric Networks. *Langmuir* **2014**, *30* (14), 4129–4136.

(26) Eidmann, G.; Savelsberg, R. The NMR MOUSE, a Mobile Universal Surface Explorer. *J. Magn. Reson. Ser. A* **1996**, *122*, 104–109.

(27) Casanova, F.; Perlo, J. *Single-Sided NMR*; Casanova, F., Perlo, J., Blümich, B., Eds.; Springer Berlin Heidelberg: Berlin, Heidelberg, 2011.

(28) Blümich, B.; Anferov, V.; Anferova, S.; Klein, M.; Fechete, R. An NMR-

MOUSE® for Analysis of Thin Objects. *Macromol. Mater. Eng.* **2003**, *288* (4), 312–317.

(29) Sharma, S.; Casanova, F.; Wache, W.; Segre, A.; Blümich, B. Analysis of Historical Porous Building Materials by the NMR-MOUSE®. *Magn. Reson. Imaging* **2003**, *21* (3-4), 249–255.

(30) Perlo, J.; Casanova, F. 3D Imaging with a Single-Sided Sensor : An Open Tomograph. **2004**, *166*, 228–235.

(31) Perlo, J.; Casanova, F.; Blümich, B. Profiles with Microscopic Resolution by Single-Sided NMR. *J. Magn. Reson.* **2005**, *176* (1), 64–70.

(32) Ghoshal, S.; Mattea, C.; Denner, P.; Stapf, S. Heterogeneities in Gelatin Film Formation Using Single-Sided NMR. *J. Phys. Chem. B* **2010**, *114* (49), 16356–16363.

(33) Merz, S.; Pohlmeier, A.; Vanderborght, J.; van Dusschoten, D.; Vereecken, H. Moisture Profiles of the Upper Soil Layer during Evaporation Monitored by NMR. *Water Resour. Res.* **2014**, *50*, 5184–5195.

(34) Yiotis, A. G.; Tsimpanogiannis, I. N.; Stubos, A. K. Fractal Characteristics and Scaling of the Drying Front in Porous Media: A Pore Network Study. *Dry. Technol.* **2010**, *28* (8), 981–990.

(35) Kaviany, M.; Mittal, M. Funicular State in Drying of a Porous Slab. *Int. J. Heat Mass Transf.* **1987**, *30* (7), 1407–1418.

(36) Prat, M. On the Influence of Pore Shape, Contact Angle and Film Flows on Drying of Capillary Porous Media. *Int. J. Heat Mass Transf.* **2007**, *50* (7-8), 1455–1468.

(37) Mujumdar, A. *Handbook of Industrial Drying*; 2006.

(38) Meiboom, S.; Gill, D. Modified Spin-Echo Method for Measuring Nuclear Relaxation Times. *Rev. Sci. Instrum.* **1958**, *29* (8), 688.

(39) Brownstein, K. .; Tarr, C. . Spin-Lattice Relaxation in a System Governed by Diffusion. *J. Magn. Reson.* **1977**, *26* (1), 17–24.

(40) Brownstein, K. R.; Tarr, C. E. Importance of Classical Diffusion in NMR Studies of Water in Biological Cells. *Phys. Rev. A* **1979**, *19* (6), 2446–2453.

(41) Song, Y.-Q. Magnetic Resonance of Porous Media (MRPM): A Perspective. *J. Magn. Reson.* **2013**, *229*, 12–24.

(42) Gomez, C. G.; Pastrana, G.; Serrano, D.; Zuzek, E.; Villar, M. a.; Strumia, M. C. Macroporous poly(EGDMA-Co-HEMA) Networks: Morphological Characterization from Their Behaviour in the Swelling Process. *Polymer (Guildf).* **2012**, *53* (14), 2949–2955.

(43) Carr, H.; Purcell, E. Effects of Diffusion on Free Precession in Nuclear Magnetic Resonance Experiments. *Phys. Rev.* **1954**, *94* (3), 630–638.

Figure 1: Scheme of a drying curve for a porous material. Four representative periods are shown: a) initial drying period, b) constant rate period, c) falling rate period and d) receding front period.

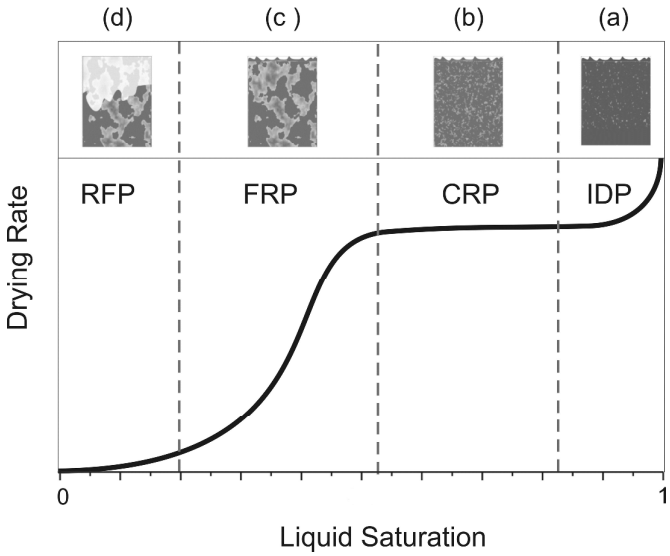

Figure 2: Schematic representation of the expected profiles during different drying dynamics. The liquid is pictured in grey and the material particles in white. The detected slices are denoted as S_i. a) Situation where evaporation proceeds from top to bottom. b) Represents a situation where evaporation is even through the whole sample and a vapour phase is developing.

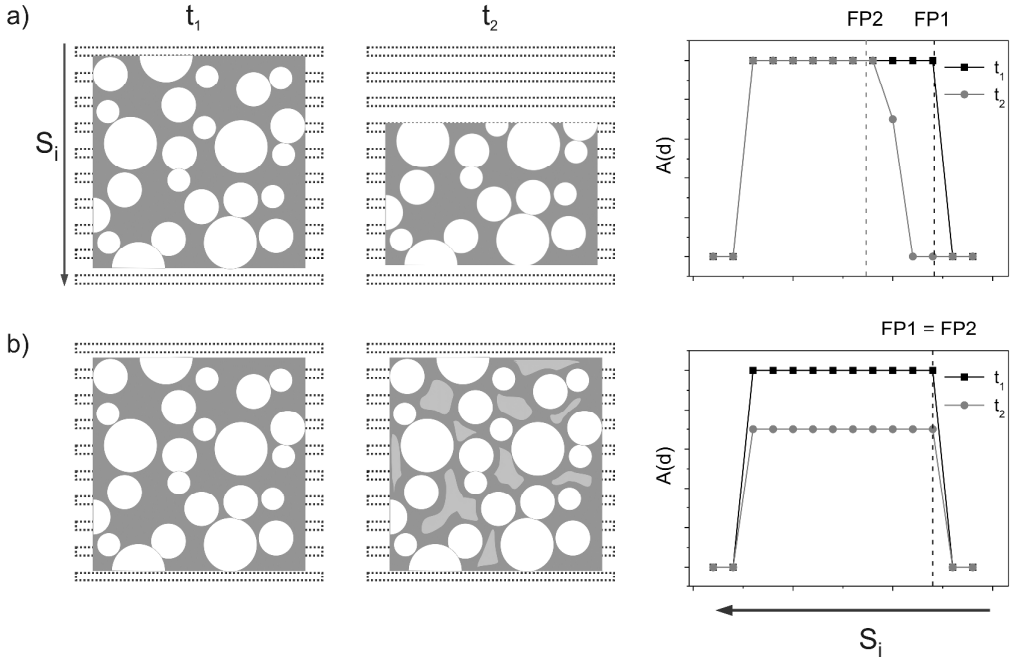

Figure 3: a) Profile obtained for a sample with 33mol-% of EGDMA fully soaked in water. b) Values of signal intensity A(0,0) for samples with different crosslinker percentage. c) Evolution of the normalized water content (nWc) during the evaporation of samples with a 33 mol % (open circles) and 6 mol % of EGDMA (black circles).

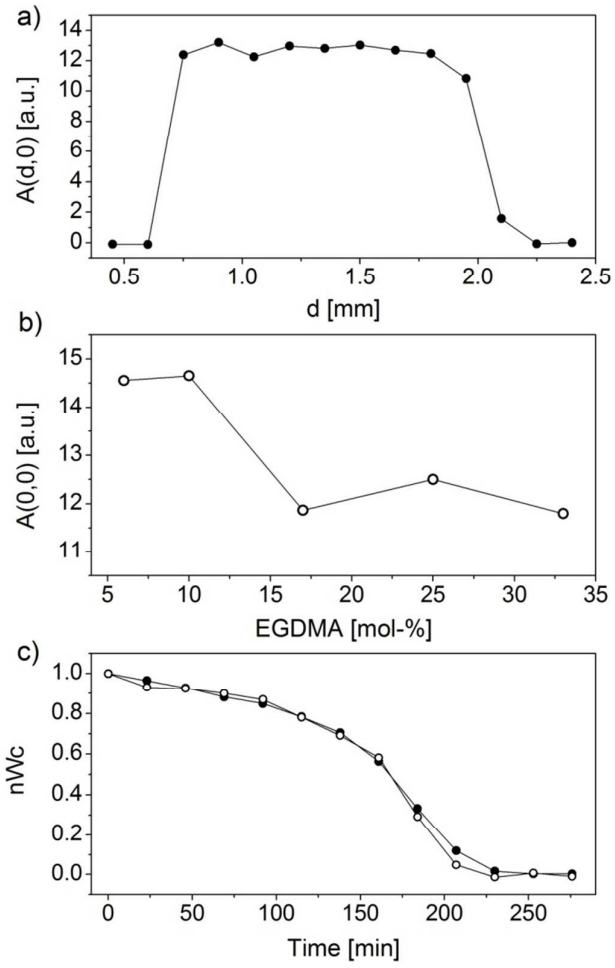

Figure 4: (color online) Profiles evolution during drying of samples with a) 33 , b) 25 , c) 17 , d) 10 and e) 6 mol % of EGDMA. Different curves were acquired with a time interval of approximately 23 minutes.

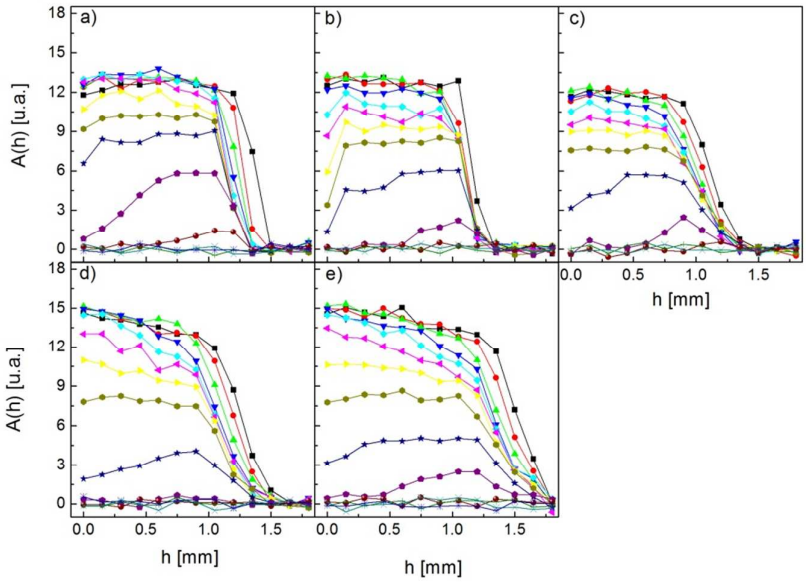

Figure 5: Evolution of the signal intensity of different slices during drying of a sample 33 mol % EGDMA content (a) and 6 % (b).

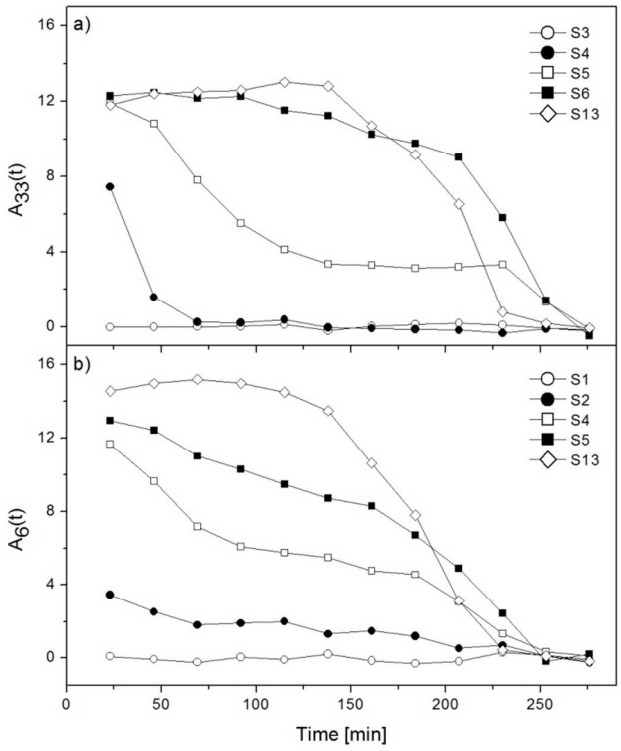

Figure 6: a) Normalized surface saturation value for different polymeric networks. b) Occurrence time of the breakthrough in terms of the samples liquid saturation value.

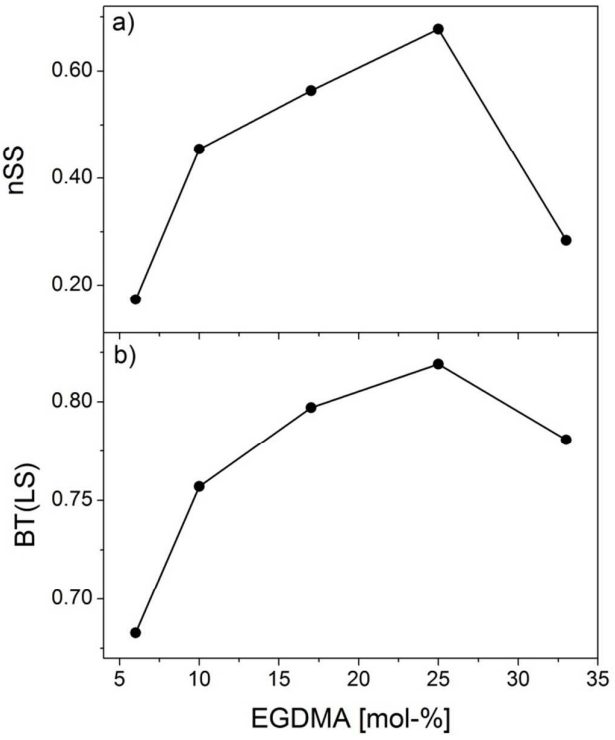

Figure 7: a) Changes in water content for the top (S5) and bottom (S13) slices of the polymer matrix with 33 mol % of EGDMA content determined by single-sided NMR. b) Evolution of the water content discriminated by pore size obtained with relaxation measurements in homogeneous 1.4 T magnetic field (data adapted from Ref. 25). Dashed lines are included as guidelines.

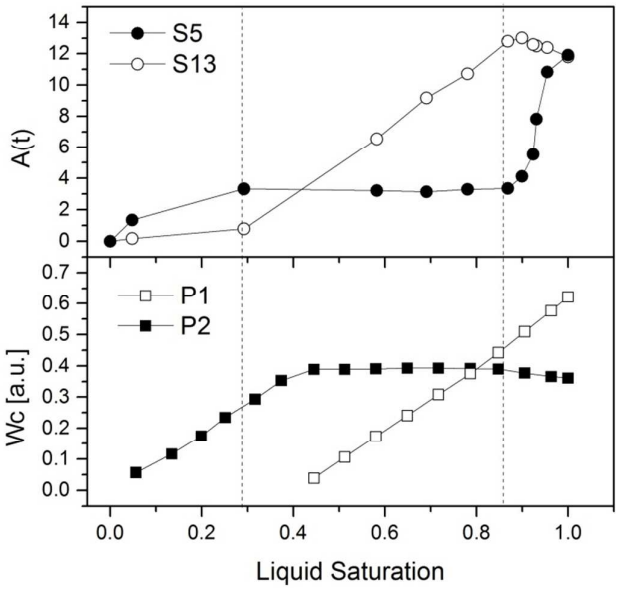

Figure 8: a) Changes in water content for the top (S5) and bottom (S13) slices of the polymer matrix with 6 mol % of EGDMA content determined by single-sided NMR. b) Evolution of the water content discriminated by pore size obtained with relaxation measurements in homogeneous 1.4 T magnetic field (data adapted from Ref. 25). Dashed lines are included as guidelines.

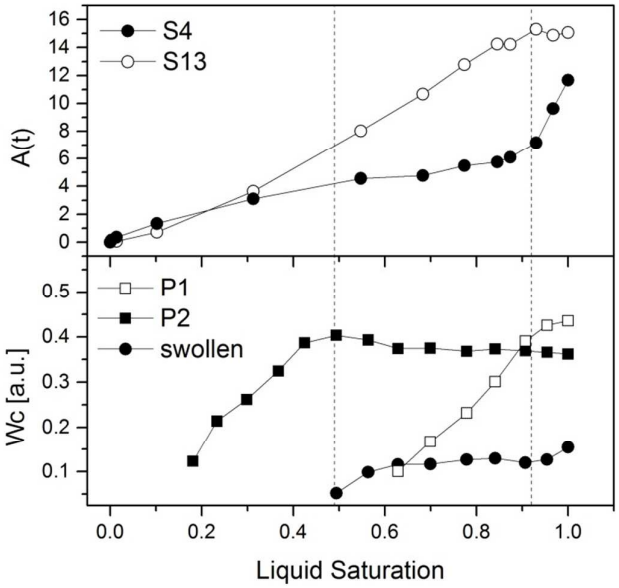

IMAGE FOR TABLE OF CONTENTS